On the nature of multiple melting in poly(ethylene terephthalate) (PET) and its copolymers with cyclohexylene dimethylene terephthalate (PET/CT)

Carlos A. Avila-Orta[a,b], Francisco J. Medellín-Rodríguez[c*], Zhi-Gang Wang[b], Dámaso Navarro-Rodríguez[a], Benjamin S. Hsiao[b,*], Fengji Yeh[b]

[a]*Centro de Investigación en Química Aplicada, Blvd. Enrique Reyna H. No. 140, Saltillo, Coah. 25100, Mexico*
[b]*Department of Chemistry, State University of New York at Stony Brook, Stony Brook, NY 11794-3400, USA*
[c]*Facultad de Ciencias Químicas, Centro de Investigación y Estudios de Posgrado, UASLP, Dr Nava No. 6, San Luis Potosí, SLP 78210, Mexico*

Abstract

The multiple melting behavior of poly(ethylene terephthalate) (PET) homopolymers of different molecular weights and its cyclohexylene dimethylene (PET/CT) copolymers was studied by time-resolved simultaneous small-angle X-ray scattering/wide-angle X-ray scattering diffraction and differential scanning calorimetry techniques using a heating rate of 2 °C/min after isothermal crystallization at 200 °C for 30 min. The copolymer containing random incorporation of 1,4-cyclohexylene dimethylene terephthalate monomer cannot be cocrystallized with the ethylene terephthalate moiety. Isothermally crystallized samples were found to possess primary and secondary crystals. The statistical distribution of the primary crystals was found to be broad compared to that of the secondary crystals. During heating, the following mechanisms were assumed to explain the multiple melting behavior. The first endotherm is related to the non-reversing melting of very thin and defective secondary crystals formed during the late stages of crystallization. The second endotherm is associated with the melting of secondary crystals and partial melting of less stable primary crystals. The third endotherm is associated with the melting of the remaining stable primary crystals and the recrystallized crystals. Due to their large statistical distribution, the primary crystals melt in a broad temperature range, which includes both second and third melting endotherms. The amounts of secondary, primary and recrystallized crystals, being molten in each endotherm, are different in various PET samples, depending on variables such as isothermal crystallization temperature, time, molecular weight and co-monomer content.
© 2002 Elsevier Science Ltd. All rights reserved.

Keywords: Poly(ethylene terephthalate); Copolymers; Melting

1. Introduction

The multiple melting behavior of semicrystalline polymers has been widely studied in the past 30 years. In particular, the linear heating of isothermally crystallized polyethylene terephthalate (PET) showed double or triple melting endotherms typically labeled as I and II or I, II and III in the order of increasing values [1–7]. The occurrence of double or triple melting behaviors in PET, as in other polymers, depends on experimental conditions, such as

temperature and time of crystallization [6], heating rate [3,6, 7], and the nature of the samples, such as molecular weight [4] and co-monomer content [5]. Triple melting behavior is typically observed when PET is crystallized at temperatures ranging between 190 and 220 °C, where endotherm II increases and endotherm III decreases with an increase of crystallization temperature. Furthermore, endotherm II is enhanced with longer crystallization times, higher heating rates, higher molecular weights and higher co-monomer contents. Two different morphological development pathways, based on experimental observations, have been proposed to explain the triple melting behavior of PET. The first pathway involves the melting–recrystallization–melting processes [2]. That is, during the heating scan, a fraction of crystals, formed during isothermal crystallization,

---

* Corresponding authors. Tel.: +1-516-631-7793; fax: +1-516-631-6518.
E-mail addresses: bhsiao@notes.cc.sunysb.edu (B.S. Hsiao), francmr@uaslp.mx (F.J. Medellín-Rodríguez).

melts at a low temperature (endotherm II); while recrystallization or reorganization occurs in the remaining fraction, thus forming crystals with higher perfection that melt at a higher temperature (endotherm III). The second pathway involves the melting of two populations of lamellar crystals [8]. In these populations, the primary lamellar crystals, formed during isothermal crystallization, melt at high temperature (endotherm III), and the secondary lamellae melt at a low temperature (endotherm II). Of course, the combination of these two pathways also offers a natural explanation to some more complicated thermal behavior.

The role of secondary crystallization in the melting behavior of PET has been widely discussed in recent years [3,9–13]. Based on the hypothesis that longer chains in homopolymers and exclusion of co-monomer moiety in copolymers may generate greater restraints to form large crystals, thus producing greater amounts of secondary crystals, Medellin-Rodriguez et al. have conducted experiments to study the triple-melting behavior of PET with different molecular weight [4] and with different co-monomer content [5]. They observed that endotherm II was enhanced when the molecular weight was increased suggesting that this endotherm is related to the melting of secondary crystals. Furthermore, endotherm III was found to be largely related to the melting of primary crystals in copolymer of poly(ethylene terephthalate *co*-1,4-cyclohexylene dimethylene terephthalate) (PET/CT), instead of the melting of recrystallized crystals, this seems to be reasonable as Yoo et al. [14] determined that the CT units are excluded from the PET crystals at CT contents lower than 20%. The rejection of CT units was considered to limit the size of the PET crystals thus, increasing the amount of secondary crystals. This phenomenon was clearly seen in the enhancement of the second melting endotherm in P(ET/CT). However, Wang et al. [6] have determined that during heating of isothermally crystallized pure PET, at moderate crystallization times (i.e. 1 h), a large amount of recrystallization or reorganization occurs. Thus the third endotherm in differential scanning calorimetry (DSC) was mainly related to the melting of recrystallized and/or reorganized material, while the second endotherm was associated to the melting of primary crystals. The recrystallization was associated to the exothermic signal, which was observed using modulated differential scanning calorimetry (MDSC) at a heating rate 2 °C/min. It is clear that there is a difference in the secondary crystallization behavior between homopolymers and copolymers, which is one of the focus in this study.

MDSC, introduced in 1993 by Reading [15], is a technique that can differentiate thermodynamic and kinetic events by means of resolving the total heat flow into reversible and non-reversible components. The reversing signal is associated with the thermodynamic events while the non-reversing signal is associated with both thermodynamic and kinetic events. Thus, MDSC is a powerful tool to study the melting of semicrystalline polymers such as PET. Recently, Sauer et al. [16] have summarized the interpretations of the MDSC traces from the melting behavior of many semicrystalline polymers. For the non-reversing melting signal, they proposed that it is due to the melting of separate lamellae or stacks of lamellae. The slower recrystallization kinetics leads to a higher non-reversing melting signal at a fixed heating rate. For the reversing melting signal, they suggested the partial melting of lamellae. These lamellae are then able to recrystallize due to the template of the melted chains and the presence of the existing crystals. Crystallization exotherms only contribute to the non-reversing signal. However, exothermic and endothermic non-reversible events can occur simultaneously.

Currently, we consider that a hybrid of the two melting mechanisms (melting–recrystallization [2] and two populations [8]) is the most probable pathway to explain the observed experimental results from the multiple melting of PET [6]. However, in order to determine the exact nature of the multiple melting in PET with different material variables, we have reinvestigated the samples with two different molecular weights and random copolymerization containing 3.5 mol% of the CT moiety. The combined characterization techniques including MDSC and simultaneous synchrotron small-angle/wide-angle X-ray scattering (SAXS/WAXS) were used to study the melting behavior and corresponding morphology changes. MDSC provided useful information about the amount of recrystallization, and SAXS was useful in determining the changes of morphological parameters and WAXS was used to determine the crystallinity during the transitions.

2. Experimental

2.1. Materials

The PET materials used in this work were obtained from Eastman Chemicals. The chosen samples were grade 9663, 10388 and 9921, with weight-average molecular weight of 55,000, 72,860, and 55,600 g/mol, respectively (subsequently denominated as LMW-PET, HMW-PET and P(ET/CT), respectively). The P(ET/CT) sample was a random copolymer of ethylene terephthalate (ET) and 1,4-cyclohexylene dimethylene terephthalate (CT), with 3.5 mol% of the CT content. The equilibrium melting point, T_m^0, of both LMW-PET and HMW-PET was about 280 °C, while the T_m^0 of P(ET/CT) was about 270.5 °C, which have been reported previously [5]. All samples were isothermally crystallized at 200 °C (after quenching from the melt) for 30 min, before heating at a rate of 2 °C/min. The supercooling for the homopolymers was 80 °C, while for P(ET/CT) was 70.5 °C. Thus, the degrees of supercooling for the homopolymer and the copolymer were

different. Also, as discussed in a previous report [5], we note that the morphological difference in the P(ET/CT) samples crystallized at 200 and 190.5 °C (supercooling equal to 80 °C) was minimum.

2.2. Conventional and modulated DSC

The thermal properties of the PET samples were measured by a TA Instruments 2920 DSC station. The temperature and the heat flow were calibrated using Indium as a standard, while the complex C_p was calibrated using Sapphire. Nitrogen atmosphere was used in all experiments. For conventional DSC experiments, the sample was first equilibrated at T_m^0 for 8 min and then rapidly cooled to 200 °C (crystallization temperature) for isothermally crystallization measurement (30 min). Subsequently, the crystallized sample was heated at a rate of 2 °C/min directly from 200 to 280 °C. For modulated DSC (MDSC) experiments, the first part of the sample treatment was the same. After the sample was cooled to 200 °C, it was isothermally crystallized at 200 °C for 25 min, and then quasi-isothermally crystallized for 5 min at a chosen modulation rate of ± 0.318 °C/min. The total crystallization time for each sample was 30 min (at iso- and quasi-isothermal conditions). In order to accomplish the desired modulation parameters and avoid possible modulation instabilities, the modulation was started before the heating scan. Finally, the sample was heated at a rate of 2 °C/min (modulation amplitude $= \pm 0.318$ °C/min) to 280 °C.

2.3. Simultaneous SAXS/WAXS

Time-resolved SAXS/WAXS measurements were carried out using two linear position sensitive detectors (European Molecular Biological Laboratory, EMBL) at the X27C beamline in the National Synchrotron Light Source (NSLS), Brookhaven National Laboratory (BNL), NY, USA. The wavelength of the X-ray was 0.137 nm, the SAXS sample to detector distance was 1428 mm and the WAXS sample to detector distance was about 150 mm. Isothermal crystallization and subsequent melting of PET samples was performed using a dual-chamber temperature jump apparatus [8]. The sample was sealed between two Kapton films. After being equilibrated for 5 min at T_m^0, the sample was rapidly jumped to a second chamber (200 °C), which was aligned in the path of the X-ray beam. The sample was held at 200 °C for 30 min and then heated to T_m^0 at a heating rate of 2 °C/min. Each SAXS/WAXS pattern was acquired at an acquisition time of 20 s. Before each run, the air scattering was measured using an empty sample holder having two Kapton films. Each X-ray profile was corrected by subtracting the air scattering. Fluctuations of the primary X-ray beam were corrected by means of an ionization chamber. Since the sample was sealed between two Kapton windows, no further correction on the sample thickness were performed.

2.4. Theoretical consideration of SAXS from semicrystalline polymers

Small-angle X-ray scattering is a powerful technique to determine the morphological features of semicrystalline polymers. Semicrystalline polymers possess alternating amorphous and crystalline layers, where the electron density of the crystalline layer (ρ_c) is larger than that of the amorphous layer (ρ_a). The SAXS contrast is directly related to the electron density difference between the two phases ($\Delta\rho(r) = \rho_c - \rho_a$). Thus the higher the contrast, the higher the scattering power. The scattering intensity can be written as [17]

$$I(q) = \Im[\Delta\rho^{*2}(r)] \tag{1}$$

where q is the scattering vector defined by $q = 4\pi/\lambda(\sin\theta)$ (λ is the wavelength and 2θ is the scattering angle), $\Delta\rho(r)$ is the local electron density deviation from the average, $\Im$ represents the Fourier transformation and ^{*2} represents the operation of autoconvolution or autocorrelation.

The evaluation of structural parameters from the SAXS data requires the access of the complete scattering data at low and high angles. However, the limits of scattering curve ($q \to 0$, $q \to \infty$) cannot be reached experimentally, the extrapolation of the scattering data has to be carried out with proper approximations. At the lower limit ($q \to 0$), a model for random phase approximation (proposed by Debye et al. [18]) can be used, which is given by

$$I(q) = \frac{A}{(1 + \varepsilon^2 q^2)^2} \tag{2}$$

where A is a constant, ε is the length of the scattering unhomogeneity. At the higher q limit ($q \to \infty$), the scattering intensity for an ideal two-phase lamellar system governed by the Porod's law [19,20] can be used ($I_{ID} = K_P/q^4$, where K_P is the Porod constant). However, due to density fluctuations within the phases [17,21–24] and a finite width interface thickness [24,25], experimental scattering data must be corrected at high q values. Thus the ideal scattering intensity should be expressed as

$$I_{ID} = \frac{I_{EXP}(q) - I_B(q)}{H^2(q)} \tag{3}$$

where $I_{EXP}(q)$ is the experimentally measured intensity, $I_B(q)$ is the background intensity due to density fluctuations and $H^2(q)$ is a smoothing function that takes into account the interface thickness. The background intensity can be considered constant [17], exponential [25] or in a power series [24], while the smoothing function can be related to sigmoidal [17] or linear [22,23] geometrical models as well as or their expanded forms. Trial and error [21] methods and non linear [4,5,26] fitting methods have often been used to extract the curve parameters.

A detailed analysis of the morphological parameters from the SAXS data can be obtained from the one-dimensional

interface distribution function, $g_1(r)$ [25]. This function is the second derivative of the one-dimensional correlation function, $\gamma_1(r)$ [27]. Experimentally, $g_1(r)$ can be obtained from

$$g_1(r) = \frac{t}{2\pi^2 V} \int_0^\infty G_1(q)\cos(qr)\mathrm{d}q \qquad (4)$$

where t is the thickness of the sample, V is the volume occupied by lamellar stacks and $G_1(q)$ is the interference function [25] given by

$$G_1(q) = \Im[g_1(r)] = K_P - q^4 I(q) \qquad (5)$$

An ideal two-phase lamellar system is necessary in order to obtain this function.

If Gaussian distributions are assumed to represent the variation of interfacial thickness, then the theoretical $g_1(r)$ function [28] can be obtained. In this case, the theoretical function $g_1(r)$ is given by

$$g_1(r) = \sum_0^\infty w_i h_i \qquad (6)$$

where w_i is the weight for the Gaussian length distributions h_i centered at r_i. The general procedure to calculate the theoretical $g_1(r)$ has been described elsewhere [5,28].

2.5. SAXS data analysis

The reciprocal-space intensity data were corrected for density fluctuations within the phases by subtracting the background intensity. The Porod's constant was calculated assuming the sharp interface boundary (interface thickness equals to zero). The corrected intensity data were extrapolated to high q values ($q = 5$ nm^{-1}) using the Porod's law [19,20] and to low q values ($q = 0.01$ nm^{-1}) using Debye's model [18]. After the extrapolations, the data were smoothed to eliminate experimental noises. The integrated intensity, invariant Q, was calculated directly from the scattered intensity at all angles. The corrected scattered intensity was then transformed into the interference function by using Eq. (5) [25] and its highest positive value was normalized to unity. The normalized reciprocal-space interference function $G_1(q)$ was then transformed into the real-space interface distribution function $g_1(r)$ using Ruland's method [25] (Eq. (4)). In order to extract the time-resolved morphological parameters from the 'experimental' $g_1(r)$, real space simulations were also performed using the finite lamellar stacking model [28] (4 lamellae per stack [29] were assumed) and the results were compared with the experimental data. The morphological parameters extracted from the best fit simulation were the crystalline thickness (l_c), amorphous thickness (l_a), long period (L) and their corresponding statistical distributions, i.e. statistical length distribution of the crystalline phase (σ_e), the amorphous phase (σ_a) and the long period (σ_L).

3. Results and discussion

3.1. Isothermal crystallization

In order to determine the nature of multiple melting behavior in PET, it is necessary to discuss the origin of primary and secondary crystals. The process of isothermal crystallization in semicrystalline polymers can be divided into two main steps [8]. The primary crystallization step characterizes the nucleation and growth of primary crystals in an unrestricted amorphous environment without the interferences on confinement of the crystals. The secondary crystallization occurs in the amorphous chains or chain segments that are restricted or interfered by the existing crystallites. Consequently, primary crystals are usually thicker because they are formed in an unrestricted space and secondary crystals are usually thinner because they are formed in a constrained space. Primary crystals thus melt at high temperatures while secondary crystals melt at low temperatures. If the thickness difference between primary and secondary crystals is significant, then two melting endotherms are observed during heating.

The overall crystallinity ϕ was obtained from the WAXS data using a general peak fitting procedure for semicrystalline polymers [30,31]. In this study, Gaussian functions were used to fit the reflection peaks as well as the amorphous background (containing two Gaussian functions). Crystallinity ϕ versus time (t) curves for the isothermal crystallization of LMW-PET, HMW-PET and P(ET/CT) are shown in Fig. 1a. It is seen that for the LMW-PET, ϕ increases sharply, while for the HMW-PET such increase is less pronounced. In the case of the P(ET/CT) the increase is rather gradual. Of course this may be due in part to the low degree of supercooling in P(ET/CT). In all three crystallinity curves, a two-step increase is clearly seen. After the first increase, the crystallization proceeds with a lesser rate indicating that secondary crystallization is now mainly taking place. The change in the slope of an Avrami plot at long times is helpful to determine if secondary crystals are formed during isothermal crystallization. The Avrami plot for each polymer is shown in Fig. 1b, where two distinct slopes characterize the different crystallization stages of LMW-PET, HMW-PET, and P(ET/CT). The first slope represents the primary crystallization and its Avrami exponent [32] (np) is about 2.5 for the three samples. The second slope represents the secondary crystallization, where the Avrami exponent (n_S) is lower and different for each sample. We consider that primary and secondary crystallization take place not in series but in a parallel manner. In other words, secondary crystallization can start well before the ending of primary crystallization. At this point, it is clear that both primary and secondary crystals are present in LMW-PET, HMW-PET and P(ET/CT) after isothermal crystallization at 200 °C. The change of morphology during heating will be discussed later.
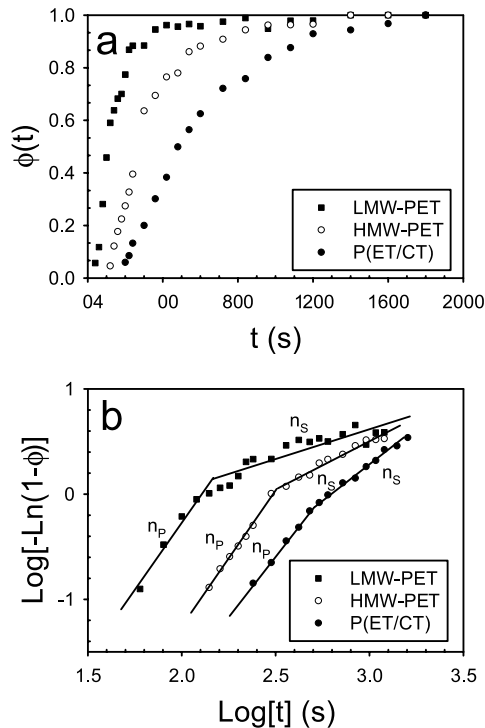
Fig. 1. Isothermal crystallization of different PET samples at 200 °C (30 min): (a) relative crystallinity, and (b) Avrami plot.

3.2. Multiple melting behavior

DSC traces of isothermally crystallized PET samples are shown in Fig. 2. It is seen that all samples show the typical triple melting behavior with endotherms labeled as I, II and III in the order of increasing melting points. Note that the endotherm I, at about 208 °C, is broad and not clearly seen. Wang et al. [6] crystallized PET of relatively low molecular weight at temperatures above 200 °C with a crystallization time of 1 h, and observed the development of the well-defined endotherm I at higher temperatures (above 220 °C). They related this endotherm with the melting of secondary crystals, while others [4,5] have speculated that this endotherm corresponds to the melting of crystals formed during the last stage of secondary crystallization. The
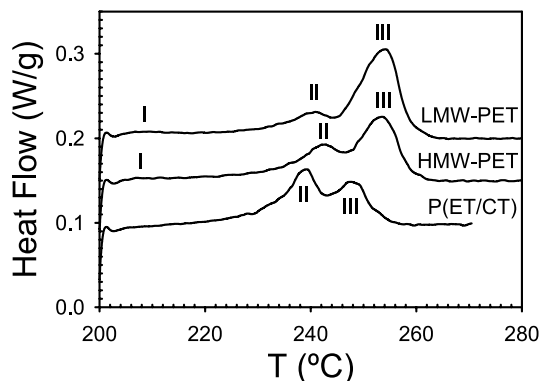

Fig. 2. DSC traces at 2 °C/min of different PET samples after isothermal crystallization at 200 °C (30 min).

second melting endotherm appears as a relatively weak peak in LMW-PET, a medium peak in HMW-PET and as a dominant peak in P(ET/CT). This melting behavior at a low heating rate (2 °C/min) clearly resembles the melting behavior at higher heating rates [4,5] (i.e. 10 °C/min) for the homopolymer, where the second endotherm is enhanced, at the expense of the third endotherm.

3.3. Morphological changes during melting

Time-resolved SAXS measurements made during heating of isothermally crystallized LMW-PET, HMW-PET and P(ET/CT) at 2 °C/min are shown in Fig. 3. Immediately after isothermal crystallization at 200 °C, a broad but distinct scattering peak is seen in all samples. The intensity of this peak is increased and the position is shifted to lower values of the scattering vector q with temperature. Above the melting point, this scattering peak disappears. In order to obtain more information from the SAXS profiles, morphological parameters, such as the amorphous and crystalline layer thicknesses and their statistical distributions, were obtained from the analysis as described in Section 2.

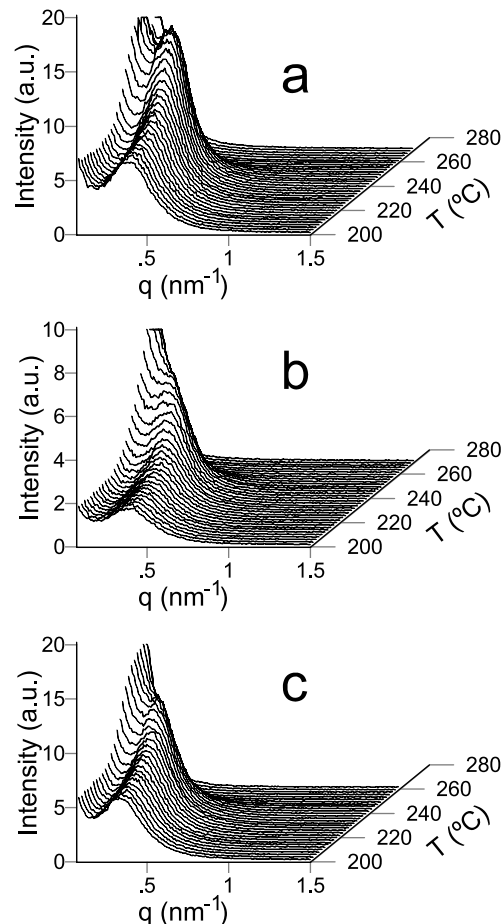It is well known that although the correlation function

Fig. 3. Time-resolved SAXS patterns during heating at 2 °C/min after isothermal crystallization at 200 °C (30 min) for (a) LMW-PET, (b) HMW-PET, and (c) P(ET/CT).

analysis can yield thicknesses of constituting layers in the lamellar structure, the assignment of the correct thickness to the amorphous or crystal layer can be ambivalent and requires verification by other measurements. This is particularly true when the crystallinity is relatively low ($<40\%$) as in this study. In an earlier SAXS study of the PET morphology, by means of the interface distribution function, $g_1(r)$, Santa Cruz et al. [33] proposed that the larger thickness is associated to the crystal phase in semicrystalline PET samples. The proposed morphology implies the existence of large amorphous regions between the lamellar stacks. These authors also concluded that the crystal thickness and the long period distributions are broad. Recently, this morphological model in PET was also confirmed by Xia et al. [29] using combined transmission electron microscopy and SAXS measurements. Their results showed that the crystal (larger) thickness has a broad distribution (the width is about 2 nm), while the amorphous thickness distribution is relatively narrow (width less than 1 nm). Wang et al. also concluded that the larger thickness from the correlation function is associated to the crystalline phase, based on the value for the volume fraction of lamellar stacks (the ratio of the mass degree crystallinity to the crystallinity within the stacks—linear crystallinity) [6,30] and the model calculation of the crystallite size along the c-axis (chain direction, D_{001}) [30].

However, there are also opposite opinions about assigning the larger thickness as the crystal thickness. The strongest evidence was provided by Ivanov et al. in a time-resolved study of isothermal crystallization of PET [34]. They found that there was no indication of thin secondary crystallites or large amorphous regions detectable by AFM. Although they measured an averaged crystal lamellar thickness in between the two thickness values calculated from the analysis of correlation function using AFM data, they chose the thinner value as the crystal thickness because AFM overestimated the crystal thickness due to the tilting of the lamellar edges and other reasons. We also agree with these authors that there are issues in AFM measurements of in situ polymer crystallization that need to be investigated further. Moreover, we caution that the direct correlation of crystallization in thin film to crystallization in polymer bulk may not be correct. As we cannot rationalize the invariant response of the crystal thickness with temperature and its relationship with the multiple melting behavior, if the smaller thickness were to assign as the crystal thickness, we decide to adhere to our original assignment. That is, the larger thickness calculated from the correlation function is related to the crystal phase and the smaller thickness is related to the interlamellar amorphous thickness. In this case, the large changes of the crystal thickness can directly mirror the multiple endothermic transitions (Figs. 4–6).

The evolution of l_a, l_c, and L, as well as their statistical distributions σ_a, σ_e, σ_L, measured during heating (2 °C/min) of isothermally crystallized LMW-PET, HMW-PET and
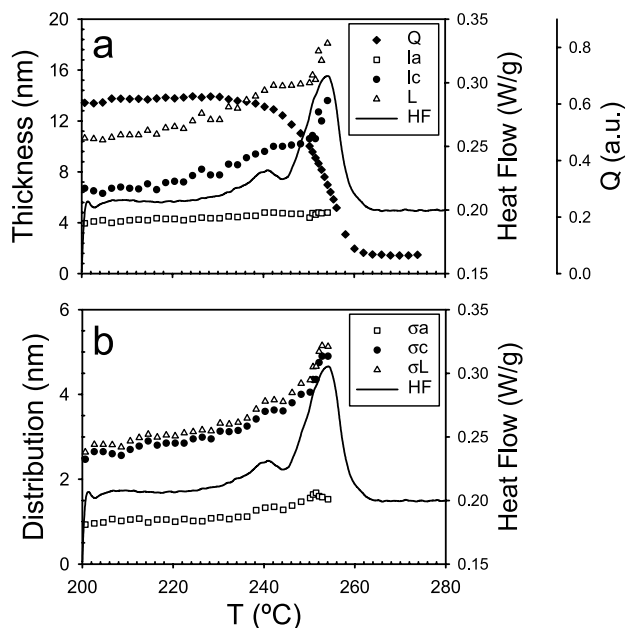

Fig. 4. Morphological changes for LMW-PET during heating at 2 °C/min after isothermal crystallization at 200 °C (30 min). (a) Lamellar thicknesses and the scattering invariant, and (b) statistical distributions of lamellar thicknesses. DSC traces are also included for comparison purpose.

P(ET/CT) are shown in Figs. 4–6, respectively. We should keep in mind that the calculated crystalline lamellar thickness, l_c, includes contributions from both primary and secondary crystals. Similarly, the calculated crystalline statistical distribution σ_c was a result of contributions of the statistical distribution from both primary and secondary crystals. In Figs. 4a, 5a and 6a it is seen that l_a for the three
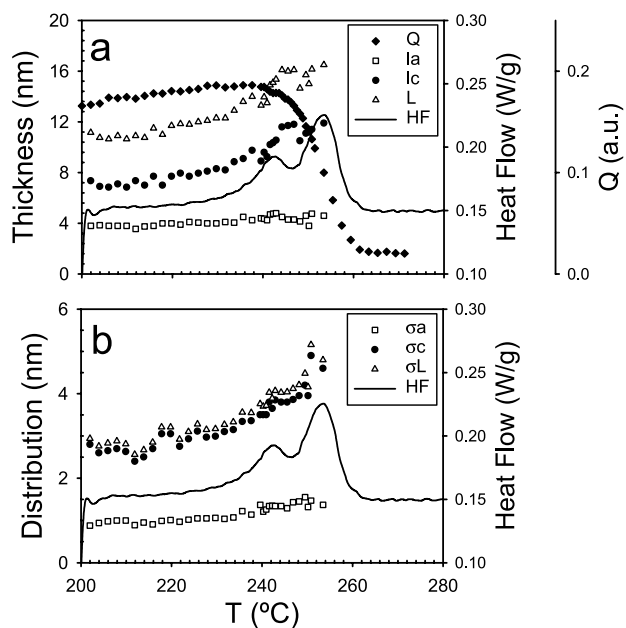

Fig. 5. Morphological changes for HMW-PET during heating at 2 °C/min after isothermal crystallization at 200 °C (30 min). (a) Lamellar thicknesses and the scattering invariant, and (b) statistical distributions of lamellar thicknesses. DSC traces are also included for comparison purpose.
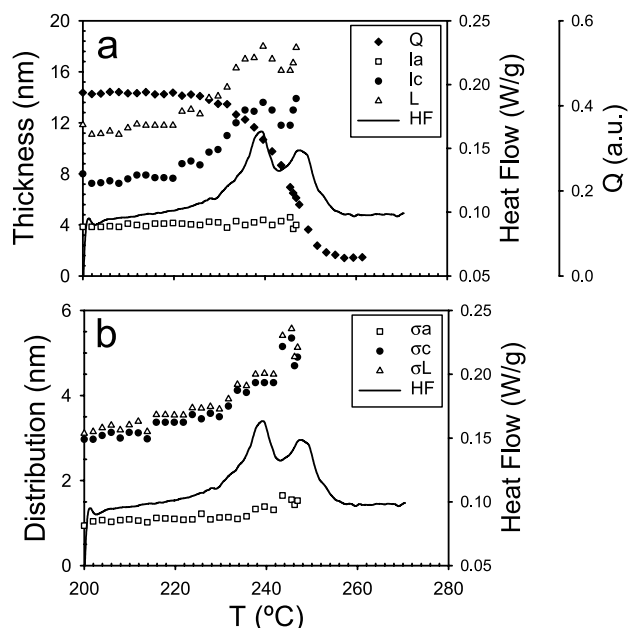
Fig. 6. Morphological changes for P(ET/CT) during heating at 2 °C/min after isothermal crystallization at 200 °C (30 min). (a) Lamellar thicknesses and the scattering invariant, and (b) statistical distributions of lamellar thicknesses. DSC traces are also included for comparison purpose.

polymers is around 4 nm and that it remains about constant through the heating scan. Since l_a is very small, the amorphous chains in the existing lamellar stacks are topologically too constrained to allow the formation of new crystals [6]. Thus, stacks of thinner lamellae are formed between the existing lamellar stacks. In Fig. 4a it is seen that l_c and L for the LMW-PET lie between 6–7 and 10–11 nm, respectively, and that these parameters show continuous increases as the temperature is increased. At temperatures where the second endotherm is present, the increases in these parameters are noticeable, and after the second endotherm these increases become more enhanced. For the HMW-PET in Fig. 5a, l_c and L are around 7 and 11 nm, respectively. It is seen that at temperatures where the second endotherm occurs, the increases in l_c and L are more pronounced in HMW-PET than those in LMW-PET. However, in HMW-PET after the second endotherm both values are decreased first and then increased considerably. In contrast in LMW-PET, there is no initial decrease and the increase is more pronounced after the second endotherm. For P(ET/CT) in Fig. 6a, l_c and L are close to 7 and 11 nm, respectively. In this copolymer, the increases in l_c and L, in the range of the second endotherm, are even higher than those in LMW-PET. After the second endotherm, l_c and L are found to decrease first and then increase later as in the case of HMW-PET. From the above results, we can conclude that the average crystalline thickness and long period generally increase with temperature for all three polymers. This phenomenon is expected in all semicrystal-line polymers, and is consistent with our assumption of the l_c and l_a. This behavior is very similar to the system of that

syndiotactic polypropylene during melting of isothermally crystallized samples [35]. The statistical distributions σ_c and σ_L are also found to increase with temperature for the three polymers as can be seen in Figs. 4b, 5b and 6b, respectively. The increase in l_c and L with temperature can be related to two different processes. One is that the original crystals can undergo a recrystallization process leading to the increases in l_c and L [2]. Second, the other is that the melting of thin crystals (i.e. secondary crystals) can result in the increase of the average sizes of crystalline thickness (the residual primary crystals have a larger thickness). To determine which process is more suitable to explain our experimental observations, we turn our attention to the MDSC results.

3.4. Recrystallization behavior during multiple melting

The total, reversing and non-reversing signals for LMW-PET, HMW-PET and P(ET/CT), measured by MDSC, are shown in Fig. 7. It should be pointed out that the total signal in MDSC is equivalent to the heat flow signal observed in conventional DSC, and for each case the conventional DSC and total MDSC signals displayed similar characteristics. In Fig. 7, the heat flow signals have been vertically shifted and
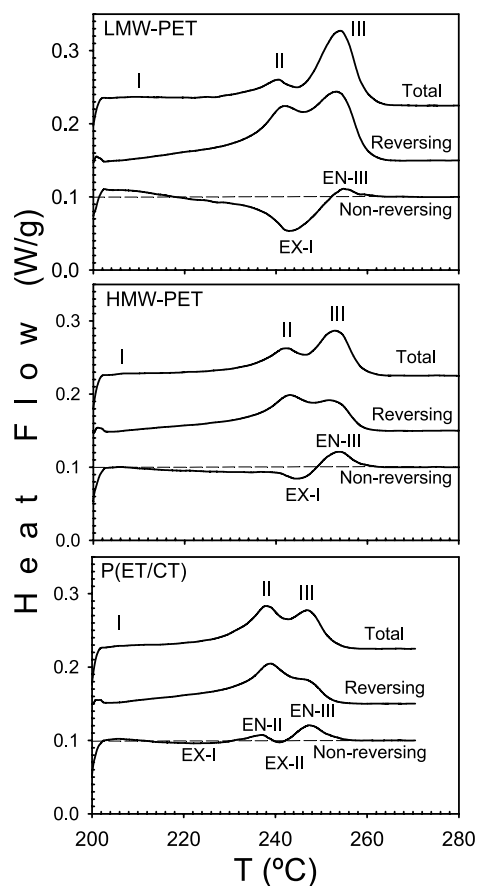

Fig. 7. MDSC traces of different PET samples after isothermal crystal-lization at 200 °C (30 min). The heating rate is 2 °C/min (the modulation amplitude = ± 0.318 °C/min).

their baselines have been slope-corrected for analysis purpose.

In Fig. 7 two melting endotherms are seen in the reversing signals of all three samples. The low temperature melting endotherm, observed in the reversing signal is labeled as II. Since its peak is close to the peak temperature of the second endotherm in the total signal; the high temperature endotherm observed in the reversing signal is labeled as III. In the reversing signal of LMW-PET, the second melting endotherm is smaller than the third one, however, in HMW-PET the second endotherm is slightly higher than the last endotherm. In P(ET/CT) the second endotherm is the dominant transition. In other words, the intensity of the second endotherm increases while the third endotherm decreases with increasing molecular weight and CT content.

The analysis of the non-reversing signal is more complicated since a series of exothermic and endothermic events have taken place during heating. However, some common features are observed in all three samples (Fig. 7). A small endotherm, located about 5 °C above the crystallization temperature, is observed for all three samples, followed by an exothermic transition. The enthalpic change associated with the exothermic transition (EX-I) is quite significant as is the case of LMW-PET (19.4 J/g), but it decreases as the molecular weight increases, HMW-PET (4.8 J/g). This exothermic transition (EX-I) is found to be significantly affected by the presence of a small amount of the CT co-monomer in P(ET/CT) (1.8 J/g). It is seen that this exothermic transition is followed by an endothermic transition (EN-III) with peak temperatures very close to the third endotherm and heat capacities of 2.1 and 4.6 J/g, in the case of LMW-PET and HMW-PET, respectively. The P(ET/CT) sample behaves slightly differently since two endothermic processes take place sequentially, one before and one after the exothermic transition. The peak of the low temperature endotherm (EN-II) is located close to the second endotherm in the total signal while the high temperature endotherm (EN-III) is located close to the final endotherm. The heat capacity of the low and high non-reversing endotherms is 1.1 and 4.3 J/g, respectively. A small exothermic event (EX-II) of 0.2 J/g is seen between these two endothermic transitions.

In order to understand the mechanics of the multiple melting behavior, the reversing and non-reversing signals were compared. Right above the crystallization temperature, all three PET samples show a small but distinct endothermic transition only in the non-reversing signal. This non-reversing endothermic transition is associated with the first melting endotherm observed in the conventional and modulated DSC. At higher temperatures, exothermic transitions, associated with the recrystallization of partially melted lamellae (observed in the non-reversing signal), take place. Sauer et al. [16] pointed out that MDSC is not completely quantitative in the characterization of the recrystallization exotherm, due to the possibility of

simultaneous occurrence of non-reversing endothermic transitions that can reduce the magnitude of the measured exotherm. However, it is clear from Fig. 7 that, even if some endothermic transitions do occur, the enthalpic change of the exotherm decreases with increasing molecular weight and CT content, indicating that the level of recrystallization for HMW-PET and P(ET/CT) is lower compared to that for LMW-PET. Furthermore, the recrystallization exotherm is proportional to the subsequent endothermic transition in HMW-PET, but it is undoubtedly not proportional to the subsequent endothermic signal in LMW-PET and P(ET/CT). This suggests that the high temperature non-reversing melting endotherm may be associated with not only the melting of crystals formed during the heating scan but also with the melting of crystals formed prior to the heating scan. In the case of LMW-PET, the heat of the non-reversing endotherm is quite small compared to the heat of the exotherm while the opposite behavior is seen in P(ET/CT). However, in LMW-PET, the heat of the non-reversing exotherm is comparable with the third reversing endotherm; while in P(ET/CT), the exotherm is quite small compared to the third reversing endotherm. Thus, the last reversing endotherm of LMW-PET should be mainly associated with the melting of recrystallized material while in P(ET/CT), the last endotherm is not directly associated with the recrystallization process.

3.5. The nature of multiple melting

The multiple melting behavior of the isothermally crystallized PET samples can in general be described as follows. From MDSC, it is seen that endotherm I is a non-reversing event, endotherm II represents the melting of crystals (both primary and secondary) formed prior to the heating scan and endotherm III is originated from the melting of both isothermally grown crystals and crystals formed during the heating scan (recrystallized material). Regarding the semicrystalline structure prior the heating scan, our SAXS results suggest the presence of two kinds of crystals (primary and secondary) intimately mixed. Therefore the calculated crystalline thickness is the result of contributions from both primary and secondary crystals. In general, the average values of l_c and L increases during heating of isothermally crystallized samples. Based on these results, we can comment on the nature of multiple melting as follows. First of all, we assume that the statistical distribution of primary crystals is broader than the distribution of secondary crystals. Consequently, while heating up to the peak temperature of endotherm II, the thin crystals melt and l_c and σ_e increase simultaneously due to the presence of dominant primary crystals. This effect is enhanced with increasing molecular weight and copolymer content due to the larger amount of both secondary crystals and/or less stable primary crystals. The partially melted polymers can recrystallize in a large temperature range after the first endotherm, whose contribution can also increase the

average crystalline thickness and its statistical distribution. The contribution of the recrystallized material is detected mainly in the third endotherm (after the second endotherm), where a sharp increase in l_c for LMW-PET and a small increase in the cases of the HMW-PET and the P(ET/CT) are seen. The recrystallized material also produces a broader statistical distribution. An increase in the molecular weight and the presence of CT in PET are less favorable to the occurrence of recrystallization processes. However, due to the initially broad statistical distribution of primary crystals, these crystals also melt at temperatures above the second endotherm. In other words, primary crystals melt in a large temperature range covering both second and third endotherms, the secondary crystals melt basically in the second endotherm range and the recrystallized material melts in the final endotherm range.

4. Conclusions

The multiple melting behavior of isothermally crystallized PET with different molecular weights and its copolymers has been studied. The origin of multiple melting has been evaluated on the basis of melting-recrystallization pathways and double crystal lamellar population. The first melting endotherm is associated with the non-reversing melting of crystals formed during the late stages of secondary crystallization. The second melting endotherm is associated with the reversing melting of secondary and partial melting of primary crystals formed prior to the DSC heating scan. The last melting endotherm is associated with a complex process of reversing and non-reversing melting. Thus the origin of the third endotherm is predominantly related to the melting of residual primary crystals formed prior to the heating scan and the melting of recrystallized material formed during the heating scan. The increase of crystalline thickness during the second endotherm is probably due to the melting of thin secondary crystals resulting in thicker primary crystals and a minor contribution of thermally thickened of primary crystals. The increase in l_c during the third endotherm is mainly associated with the presence of crystals formed during the heating scan. It was found that the statistical distribution of primary crystals is broad compared to the distribution of secondary crystals. The statistical distribution increases during heating due to the melting of secondary crystals and the formation of new recrystallized crystals. The amount of secondary crystals affects greatly the enthalpic change of the second endotherm while the amount of recrystallized material is one of the major effects on the third melting endotherm. As LMW-PET can easily be recrystallized, its third endotherm is more enhanced. Since P(ET/CT) has a great amount of secondary crystals, its second melting endotherm becomes dominant. Finally, we note that the melting behavior in HMW-PET shows an intermediate behavior between LMW-PET and P(ET/CT).

References

[1] Roberts RC. Polymer 1969;10:117.
[2] Roberts RC. J Polym Sci, Polym Lett 1970;8:381.
[3] Zhou C, Clough SB. Polym Engng Sci 1988;28:65.
[4] Medellín-Rodríguez FJ, Phillips PJ, Lin JS, Campos R. J Polym Sci, Polym Phys 1997;35:1757.
[5] Medellín-Rodríguez FJ, Phillips PJ, Lin JS, Avila-Orta CA. J Polym Sci, Polym Phys 1998;36:763.
[6] Wang Z-G, Hsiao BS, Sauer BB, Kampert WG. Polymer 1999;40:4615.
[7] Medellín-Rodríguez FJ, Phillips PJ. Macromolecules 1995;28:7744.
[8] Basset DC, Olley RH, Al Raheil RAH. Polymer 1988;29:1745.
[9] Groeninckx G, Reynaers H, Berghmans H, Smets G. J Polym Sci, Polym Phys 1980;18:1311.
[10] Lee Y, Porter RS. Macromolecules 1987;20:1336.
[11] Holdsworth PJ, Turner-Jones A. Polymer 1971;12:195.
[12] Fontaine F, Ledent J, Groeninckx G, Reynaers H. Polymer 1982;23:185.
[13] Zachmann HG, Stuart HA. Makromol Chem 1960;41:148.
[14] Yoo HY, Umemoto S, Kikutani T, Okui N. Polymer 1994;35:117.
[15] Reading M. Trends Polym Sci 1993;1:248.
[16] Sauer BB, Kampert WG, Blanchard EN, Threefoot SA, Hsiao BS. Polymer 2000;41:1099.
[17] Ruland W. J Appl Crystallogr 1971;4:70.
[18] Debye P, Anderson Jr. HR, Brumberger H. J Appl Phys 1957;28:679.
[19] Porod G. Kolloid Z-Z Polym 1951;124:83.
[20] Porod G. Kolloid Z-Z Polym 1952;125:51.
[21] Siemman U, Ruland W. Colloid Polym Sci 1982;260:999.
[22] Blundell DJ. Acta Crystallogr 1970;A26:472.
[23] Blundell DJ. Acta Crystallogr 1970;A26:476.
[24] Vonk CG. J Appl Crystallogr 1973;6:81.
[25] Ruland W. Colloid Polym Sci 1977;255:417.
[26] Hsiao BS, Verma R. J Synchrotron Rad 1997;5:23.
[27] Vonk CG, Kortleve G. Kolloid Z-Z Polym 1967;220:19.
[28] Stribeck N, Ruland W. J Appl Crystallogr 1978;11:535.
[29] Xia Z, Sue H-J, Wang Z-G, Avila-Orta CA, Hsiao BS. J Macromol Sci, Phys 2001;B40:625.
[30] Wang Z-G, Hsiao BS, Fu X, Liu L, Yeh F, Sauer BB, Chang H, Schultz JD. Polymer 2000;41:1791.
[31] Balta-Calleja FJ, Vonk C. X-ray scattering of synthetic polymers. New York: Elsevier; 1989.
[32] Avrami M. J Chem Phys 1939;7:1103.
[33] Santa Cruz C, Stribeck N, Zachmann HG, Balta-Calleja FJ. Macromolecules 1991;24:5980.
[34] Ivanov DA, Amalou Z, Magonov SN. Macromolecules 2001;34:8994.
[35] Wang ZG, Wang XH, Hsiao BS, Phillips RA, Medellín-Rodríguez FJ, Srivatsan S, Han CC. J Polym Sci, Part B: Polym Phys 2001;39:2982.